A Classification Approach to Recognize the Firing of Spinal Motoneurons in Amyotrophic Lateral Sclerosis

Amr Y. Abdelaal, Mohamed H. Mousa, Mai Gamal, Mahmoud I. Khalil, Sherif M. Elbasiouny, and Seif Eldawlatly

***Abstract*— Amyotrophic Lateral Sclerosis (ALS) is a fatal neurodegenerative disease that affects the nervous system causing muscle weakness, paralysis, leading to death. Given that abnormalities in spinal motoneuron (MN) excitability begin long before symptoms manifest, developing an approach that could recognize fluctuations in MN firing could help in early diagnosis of ALS. This paper introduces a machine learning approach to discriminate between ALS and normal MN firing. The approach is based on two electrophysiological markers; namely, spiking latency and the spike-triggered average signal. The method is examined using data generated from a computational model under systematic variation of MN properties. Such variations mimic the differential dynamic changes in cellular properties that different MN types experience during ALS progression. Our results demonstrate the ability of the approach to accurately recognize ALS firing patterns across the spectrum of examined variations in MN properties.**

***Clinical Relevance*— These results represent a proof of concept for using the proposed machine-learning approach in early diagnosis of ALS.**

I. Introduction

Amyotrophic Lateral Sclerosis (ALS) causes rapid progressive degeneration of upper and lower motoneurons (MNs) [1]. The common symptoms of ALS are muscle weakness and fasciculations, and symptoms of dyspnea and dysphagia develop in later stages of the disease [1]. Importantly, more than half of the patients die within the first 30 months and only 20% of the patients survive between 5 and 10 years after symptom onset. One of the most critical challenges with ALS is the difficulty of making an early and accurate diagnosis. Because there is no specific criterion for ALS diagnosis in clinical practice, ALS is diagnosed by exclusion criteria. This elongates the duration between the onset of symptoms and diagnosis reaching on average 13–18 months [1].

ALS pathogenesis involves numerous changes in the cellular properties of MNs, leading to changes in their firing activity [2]. Importantly, ALS affects the three types of MNs unequally: the Slow-twitch fatigue resistant (S) cells are the most resistant to the disease, the fatigue-resistant (FR) cells are more vulnerable, whereas the fast-twitch fatigable (FF) cells are the most vulnerable in the disease [3]. The change in MN soma size is one example of the differential alterations that occur across MN types early in ALS, in which disease-vulnerable MNs (FR and FF types) were found to exhibit increased soma size unlike the disease-resistant MNs (the S type) [2]. Given these differential changes, the examination of firing properties of MN types could thus assist in early ALS diagnosis.

In this paper, we propose a machine learning approach that aims – as a proof-of-concept – to detect the fluctuations in MN excitability as ALS progresses based on nerve activity. We examined the performance of the developed classification approach on simulated data generated from a high-fidelity computational model that simulates the MNs' activity of the cat medial gastrocnemius (MG) muscle [4]. The model simulated the cellular changes recorded experimentally in each MN type in early ALS pathogenesis, some of which are disease changes while others are compensatory. Because it is unknown how these changes develop during early disease pathogenesis (i.e., separately or concurrently), we simulated them in the model individually and in combinations and analyzed each condition using the developed classification technique. We analyzed the firing activity at three levels: 1) MN pool activity, 2) MN-type activity, and 3) individual MN cells activity. Our results demonstrate the high potential of our proposed approach in differentiating between the control and the ALS conditions.

This work is supported by 1) the National Academy of Sciences (NAS, Subaward No: 2000009148), the United States Agency for International Development (USAID) and Science and Technology Development Fund (STDF) – US-Egypt Joint Science and Technology Research Collaboration Program grant # USC18-1082, 2) the U.S. National Institute of Neurological Disorders and Stroke grant # NS091836, and 3) the Google PhD fellowship program. Any opinions, findings, conclusions, or recommendations expressed in this article are those of the authors alone, and do not necessarily reflect the views of USAID or NAS.

A. Y. Abdelaal is with the Computer and Systems Engineering Department, Faculty of Engineering, Ain Shams University, Cairo, Egypt (e-mail: G16091555@eng.asu.edu.eg) – first co-author.

M. H. Mousa is with the Department of Biomedical, Industrial, and Human Factors Engineering, College of Engineering and Computer Science, Wright State University, Dayton, OH, United States (e-mail: mohamed.mousa@wright.edu) – first co-author.

M. Gamal is with the Computer Science and Engineering Department, Faculty of Media Engineering and Technology, German University in Cairo, Cairo, Egypt (e-mail: mai.tharwat@guc.edu.eg).

M. I. Khalil is with the Computer and Systems Engineering Department, Faculty of Engineering, Ain Shams University, Cairo, Egypt (e-mail: mahmoud.khalil@eng.asu.edu.eg).

S. M. Elbasiouny is with the Department of Neuroscience, Cell Biology, and Physiology, Boonshoft School of Medicine and College of Science and Mathematics, and the Department of Biomedical, Industrial, and Human Factors Engineering, College of Engineering and Computer Science, Wright State University, Dayton, OH, United States (phone: 937-775-2492; fax: 937-775-3391, e-mail: sherif.elbasiouny@wright.edu) – corresponding author.

S. Eldawlatly is with the Computer and Systems Engineering Department, Faculty of Engineering, Ain Shams University, and Faculty of Media Engineering and Technology, German University in Cairo, Cairo, Egypt (e-mail: seldawlatly@eng.asu.edu.eg).

II. METHODS

A. Model

The multi-scale, high-fidelity computer model of the spinal MN pool innervating the MG muscle we published in [4] was used to simulate the firing behaviors of MNs under normal and ALS conditions. This pool model has 51 model cells with full representation of the anatomical and electrical properties of different MN types: S (13 cells), FR (13 cells), and FF (25 cells) types, which have different vulnerability in ALS. Each model cell has somatic and dendritic ion channels that allow simulating the firing behaviors of MN types.

Experimentally, a number of early (P10) cellular changes have been measured in G93A MNs long before symptom onset at P90: 1) soma size increase [2], 2) Ca persistent inward currents increase [5], and 3) SK currents reduction (unpublished data). Thus, to simulate ALS cellular changes, each of these changes have been included in the model with the same magnitude measured experimentally, one at a time and in combinations, to give the following conditions: *ALS #1*: Increased soma size of FR and FF MNs, *ALS #2*: Increased Ca^{2+} current of all MNs, *ALS #3*: Reduced SK current of FR and FF MNs, *ALS #4*: ALS #1 and #2 conditions combined, *ALS #5*: ALS #1 and #3 conditions combined, *ALS #6*: ALS #2 and #3 conditions combined, and *ALS #7*: ALS #1, #2, and #3 conditions combined. *WT*: control condition representing the normal state where model MN properties were unchanged.

B. Data Preprocessing

The data generated from the computational model includes extracellular recordings of pool activity, extracellular recordings of each MN type activity, and the spike trains of 51 MN cells. Accordingly, we generated spike trains for both pool activity and MN-type activity, from the extracellular recordings. Two steps are involved in the generation of spike trains from extracellular recordings. The first step is the detection of compound action potentials (coAPs) generated as a result of each stimulus trigger in the data. The second step is generating a spike at the peak of each detected coAP. The detection step starts by determining the beginning of the coAP, which is assumed to be the time instant of the stimulus onset. We then identify the peak of the coAP in a 5ms interval from the stimulus onset [6]. The coAP duration is set as $2 \times (t_p - t_s)$, where t_p is the time instant at which the peak of coAP occurs and t_s is the stimulus onset. The durations of all detected coAPs are then unified to have the longest coAP duration. The step of spike train generation is implemented by creating a zero vector with the same length of the extracellular signal, and then ones are inserted at the time instants of the detected peaks (spikes).

C. Spike Train Markers

Spike trains are analyzed by examining two electrophysiological markers. The first marker is the spiking latency, which is the time interval between each spike and the onset of the immediately preceding stimulation pulse [7]. The second marker is the Spike-Triggered Average (STA), which represents the stimulus signal preceding each spike averaged across a number of stimulation pulses computed as [8]

$$STA = \frac{1}{n} \sum_{i=1}^{n} y_i \qquad (1)$$

where n is the number of pulses considered in the average, y_i is a window of the stimulation vector corresponding to the time interval ending by the timestamp of spike i.

D. Classification Approach

Our first step in the classification task is to split each spike train into fixed-size 200ms segments. Latency and STA are extracted from each segment, where each segment represents a single data point. Principal Components Analysis (PCA) is then applied to all data points [9]. We employ PCA as a dimensionality reduction step to find a better representation of the data neglecting the components with the least variability.

The next step is the classification stage in which we perform binary classification between the wild-type (WT) and each ALS case using Support Vector Machine (SVM) classifier. SVM is a supervised classification technique which is based on searching for a hyperplane with the maximum margin among the support vectors that can be achieved by minimizing the following objective function [10]

$$J = \sum_{i=1}^{l} \alpha_i - \frac{1}{2} \sum_{i=1}^{l} \sum_{j=1}^{l} \alpha_i \alpha_j y_i y_j K(x_i, x_j) \qquad (2)$$

where x_i is an input vector, y_i is a class label, α_i is a Lagrange multiplier, K is the kernel function, and l is the total number of input vectors. In our work, we used the radial basis kernel.

In our analysis, we performed 150-fold cross-validation where data points are divided by the ratio of 90% for training and 10% for testing. The points selection for training/testing is randomized over each fold. The performance of the approach is assessed using the classification accuracy computed for the testing datasets averaged across the 150 folds.

III. RESULTS

A. Dataset and Extracted Markers

The spiking behavior of different ALS conditions versus WT was investigated by running a 5-second-long simulation over 51 model MNs. To simulate ventral root electrical stimulation, the modeled MNs were stimulated via 100 stimuli of synchronous synaptic activation of 25Hz and 1ms stimulation frequency and time, respectively. Consequently, a single coAP is elicited for every synaptic stimulus in which ALS firing was observed to lag WT firing (Fig. 1a). The coAP signal was further analyzed to generate the pool firing in which a spike is detected for each coAP (Fig. 1b). Thus, each spike represents the total activity of the underlying 51 cells population. The figure demonstrates the lag in firing of the ALS pool compared to WT.

Given that ALS affects MN types differently, we also analyzed the spike trains of each cell type (S, FR and FF). Fig. 1c illustrates the MN-type spiking in which the spiking of all neurons corresponding to each type is represented with a single spike. These spikes were extracted from the coAP of each MN type computed in the model. The final level of our analysis examined spiking of each of the 51 model cells separately. Fig. 1d illustrates the spiking of a sample set of the first 5 cells for each type in which fast cells fire before small cells consistent with electrical stimulation reversed recruitment of MNs [11]. Consistent with the observations in Fig. 1a-c, a significant difference in individual cells' firing time could be seen in ALS vs. WT.

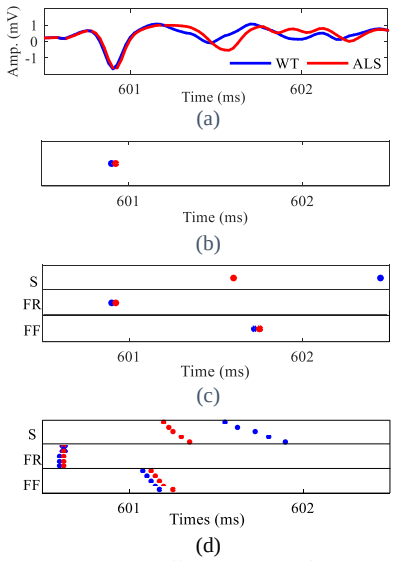

Figure 1. Outline illustrating different levels of data analysis. (a) coAP recording in response to 1 synaptic activation stimulus for WT (blue) and ALS (red). (b) Pool spikes. (c) MN-type spikes. (d) Sample single cell spikes.

In our work, we have investigated Peristimulus Time Histogram (PSTH), Inter-Spike Interval (ISI) histogram, Spiking latency and STA for each ALS condition followed by the classification technique to discriminate between ALS and WT datasets. However, we are reporting here the results of the latency and STA markers only given the significant effect different ALS conditions had on them compared to the PSTH and ISI. Fig. 2 illustrates the mean spiking latency for pool firing (Fig. 2a), MN-type firing (Fig. 2b), and single cell firing (Fig. 2c). The largest difference in spiking latency seen in the pool firing was between WT vs. ALS #1 and ALS #5 conditions (Fig. 2a, ~0.025ms). A difference in latency was also seen between the pool firing of WT vs. most of the other ALS conditions, but not as strong. Larger differences emerged at the MN-type and single cell firing levels. For instance, the difference in latency between the firing of S MN-type in WT vs. ALS #6 condition was 0.81ms (Fig. 2b). At the single cell level, a difference in latency of 14.69ms was observed in the firing of the 13th S cell in WT vs. ALS #6 condition.

ALS cellular changes also had a clear impact on the extracted STA of the pool firing (Fig. 3a), MN-type firing (Fig. 3b), and single cell firing (Fig. 3c). The variations can be mainly observed in the first time instant at which the STA reaches its peak value (i.e. first-peak time). Similar to the variations in latency, more differences in STA first-peak time could be observed at the MN-type firing and single cell firing as illustrated in Fig. 3b and Fig. 3c, respectively, compared to the pool firing (Fig. 3a). For instance, the mean difference in first-peak time between WT and ALS #3 condition is 1.2ms. In sum, the above data suggest that spiking latency and STA features could be used as markers to differentiate between WT and ALS conditions from firing behaviors.

B. Pool Firing Analysis

We first examined the performance of the classification approach when analyzing the pool firing. Each single spike in the pool firing represents the total pool activity of all 51 MNs combined for each stimulation pulse. These spikes were analyzed by extracting the latency and STA markers. STA-computed markers were then fed to PCA for dimensionality reduction and better representation. The projections on the first two principal components were finally provided to the SVM classifier for classification. For the latency, given that it represents a single dimensional data in this case, it was provided directly to the classifier.

Fig. 4 illustrates the mean accuracy over multiple cross-validation folds, where the data points were shuffled among the training and testing datasets. The figure demonstrates the performance of the approach in discriminating between WT and all ALS conditions. The increase in soma size (ALS #1 condition) had the largest mean accuracy of 98 ± 2.8% and 95± 6.2% for the latency and STA markers, respectively. The mean classification accuracy was also >95% for ALS condition #5 using both markers. In terms of differences in performance, a statistical significance, yet not consistent, is observed in most of the conditions as shown in Fig. 4 comparing the accuracy achieved for latency versus STA. The mean accuracy across all conditions was 65 ± 7.1% for latency and 68 ± 10.9% for STA markers.

While high accuracy was achieved for some ALS conditions, lower accuracy was observed for other conditions, such as ALS #4 condition as shown in Fig. 4. This poor performance could be explained by the counter-effects caused by these conditions on MN firing. For instance, ALS #1 condition leads to increased firing latency for the ALS pool

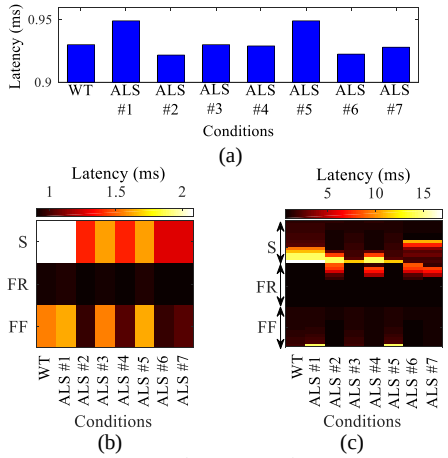

Figure 2. Mean spiking latency for (a) pool firing, (b) MN-type spikes, and (c) single cell spikes under different conditions.

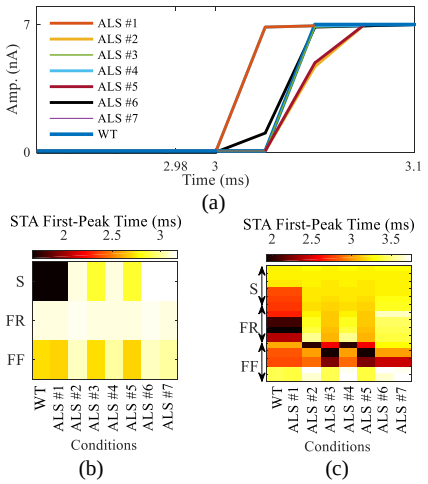

Figure 3. Average STA of (a) pool firing, (b) peak time computed for MN-type spikes, and (c) peak time computed for single cell spikes.

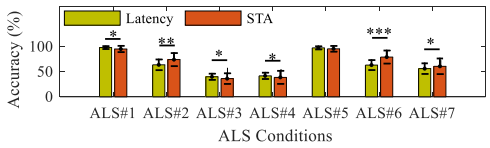

Figure 4. Classification accuracy for pool firing analysis for different conditions using both the latency and STA markers. *P < 0.05, **P < 1e-10, ***P < 1e-20, Wilcoxon rank-sum test.

compared to WT, whereas ALS #2 leads to a decreased latency (Fig. 2a). As a result, a net effect of no significant change in ALS pool firing latency vs. WT might be observed. Therefore, further analysis is required to be able to discriminate between ALS and WT cases in these conditions.

C. MN-Type Firing Analysis

Given the performance drop observed in some conditions when analyzing the pool firing, we next investigated whether analyzing the activity of each MN type could succeed in achieving higher classification accuracy. We hypothesized that such analysis would result in better performance given the differential vulnerability different cell types have in ALS. In this analysis, the coAP of each MN type generated from the model was used. Three spike trains are then obtained corresponding to the three MN types, where each spike represents the activity of all cells of each type. The entire process of feature extraction, PCA and SVM was then applied.

Fig. 5 shows the mean classification accuracy over multiple cross-validation folds of MN-type data points for training and testing sets. The figure demonstrates an overall better performance compared to the pool firing case for the ALS #3 and ALS #4 conditions. A mean accuracy of 97.63 ± 3.1% and 97.07 ± 3.08% is achieved for ALS #3 and ALS #4 conditions using the latency marker, respectively. By identifying the maximum mean accuracy achieved for each ALS condition and averaging across all conditions, a mean accuracy of 98.63 ± 1.93% and 97.9 ± 3.73% was achieved for the latency and STA markers, respectively. This indicates that using MN type-based spike trains outperforms using the pool firing markers as input to the classification technique.

D. Single Cells Firing Analysis

We finally analyzed the performance of the classification approach when applied to single cell firing. In this case, spike trains of all 51 cells were used to extract the latency and STA markers. Fig. 6 illustrates the mean classification accuracy over multiple cross-validation folds. In this figure, the accuracy achieved for the cells of the same type was averaged across cells. The figure shows comparable performance to that achieved for MN type firing analysis with a mean accuracy across all conditions of 97.94 ± 2.84% and 96.45 ± 5.54% for the latency and STA markers, respectively. It should be noted though that decomposing the coAP to extract the firing of each of the 51 cells using current state-of-the-art decomposition methods is challenging in practice.

IV. Conclusion

We introduced a classification approach that could differentiate between WT vs. ALS motoneuron firing patterns. Our analysis identified two electrophysiological markers that could be used to discriminate between the two cases, which are the spiking latency and STA. Our results demonstrated the ability of the classification approach to classify the extracted

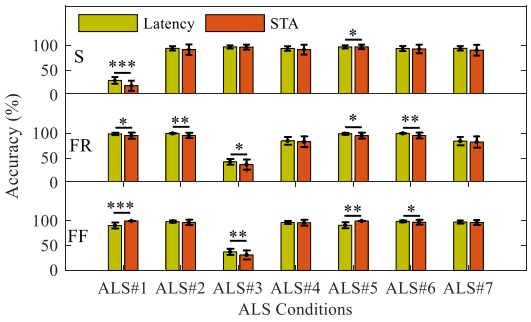

Figure 5. Classification accuracy for MN-type spiking analysis for different conditions using both the latency and STA markers. *P < 0.05, **P < 1e-10, ***P < 1e-20, Wilcoxon rank-sum test.

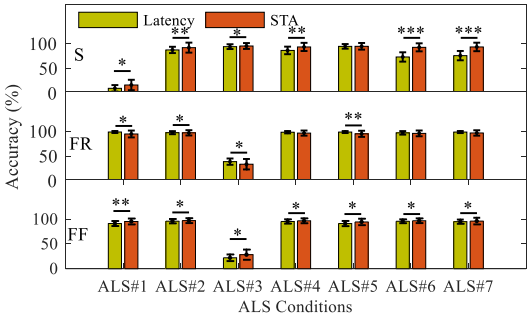

Figure 6. Classification accuracy for single cell firing analysis for different conditions using both the latency and STA markers. *P < 0.05, **P < 1e-10, ***P < 1e-20, Wilcoxon rank-sum test.

markers with a ~99% accuracy in many cases. No significant difference in the accuracy was observed between the two markers. These results indicate that the proposed approach could open new realms for accurate early ALS diagnosis that ought to be verified using animal and/or human data.

References

[1] S. Zarei, *et al.*, "A comprehensive review of amyotrophic lateral sclerosis," *Surgical neurology international*, vol. 6, 2015.

[2] S. S. Dukkipati, *et al.*, "The vulnerability of spinal motoneurons and soma size plasticity in a mouse model of amyotrophic lateral sclerosis," *The Journal of physiology*, vol. 596, pp. 1723-1745, 2018.

[3] K. C. Kanning, *et al.*, "Motor neuron diversity in development and disease," *Annual review of neuroscience*, vol. 33, pp. 409-440, 2010.

[4] J. M. Allen and S. M. Elbasiouny, "The effects of model composition design choices on high-fidelity simulations of motoneuron recruitment and firing behaviors," *Journal of neural engineering*, vol. 15, p. 036024, 2018.

[5] K. A. Quinlan, *et al.*, "Altered postnatal maturation of electrical properties in spinal motoneurons in a mouse model of amyotrophic lateral sclerosis," *The Journal of physiology*, vol. 589, pp. 2245-2260, 2011.

[6] M. S. Lewicki, "A review of methods for spike sorting: the detection and classification of neural action potentials," *Network: Computation in Neural Systems*, vol. 9, pp. R53-R78, 1998.

[7] K. Kryściak, *et al.*, "Changes in motor unit properties in SOD1 (G93A) rats," *Muscle & nerve*, vol. 50, pp. 577-586, 2014.

[8] E. Chichilnisky, "A simple white noise analysis of neuronal light responses," *Network: Computation in Neural Systems*, vol. 12, pp. 199-213, 2001.

[9] H. Abdi and L. J. Williams, "Principal component analysis," *Wiley interdisciplinary reviews: computational statistics*, vol. 2, pp. 433-459, 2010.

[10] C. Cortes and V. Vapnik, "Support-vector networks," *Machine learning*, vol. 20, pp. 273-297, 1995.

[11] J. T. Mortimer, "Motor prostheses," in *Handbook of Physiology: The Nervous System*, V. B. Brooks, Ed., ed Bethesda, MD: Amer. Physiol. Soc., 1981, pp. 155-187.